First-principles calculations to investigate structural, electrical, and optical properties of half Heusler alloy LiCrN

Ammar A. Kadhim [a], Jabbar M. Khalaf Al-zyadi [b],*, Maged A. Nattiq [b]

[a] *Department of Chemistry, College of Education/Qurna, University of Basrah, Basrah 6100, Iraq*
[b] *Department of Physics, College of Education for Pure Sciences, University of Basrah, Basrah 6100, Iraq*

A B S T R A C T

It is important in spintronics to find high performance materials that can be employ in this field. Based on the density functional theory (DFT), first principles calculations are utilized to inspect the structural, electrical and optical features of half Heusler structure LiCrN. The equilibrium lattice constant is equal to 5.11 Å. The electronic structure results display that the alloy LiCrN shows a half-metallic property. It appears that this structure has semiconductor property with an indirect band gap of 3.65 eV in (PBE-GGA) and 5.06 eV in (HSEO6) in spin down channel and the other spin channel has metallic property. The Cr atom is more effective than the other elements in this material as it carries more valence electrons in outer shell. The spin polarization shows 100% at the Fermi-level. According to Slater–Pauling rule ($Z_t - 8$), the total magnetic moment equals 4 μ_B. Additionally, we study the optical properties as we have semiconductor property in one of spin channels so it can be a candidate in optoelectronic devices. The results appear that this structure is promising in spintronics potential applications.

© 2022 Elsevier B.V. All rights reserved.

1. Introduction

The most attractive prospects for spintronics materials are half-metallic ferromagnetic (HMF), which shows metallicity only in a single spin states out of each two and are expected to have a spin polarization (SP) of 100% around the Fermi level (E_F) [1]. The Heusler alloys exhibit metal and semiconductor properties in the spin-up and spin-down channels, respectively. De Groot et al. were the first to recognize half-metallic ferromagnetism as a fact in NiMnSb in 1983 [2]. Until far, various kinds of compounds have been discovered to be HMF, including full-Heusler compounds [3–11], rutile-kind [12], spinel [13], pyrite structure [14], double perovskite and perovskite [15,16], and some diluted magnetic semiconductors [17–20]. Half Heusler alloys with half-metallic properties and high spin polarization at Fermi level consist of LiMnZ (Z = N, P, Si) [21], XCrZ (X = Li, K, Rb, Cs, Z = S, Se) [22], MnVZ (Z = P, As, Sb) [23], NaZrZ (Z = P, As, Sb) [24], RhCrZ (Z = Si, Ge) [25], NiTiX and CoVX (X= Sb and Sn) [26], CoCrZ (Z = Al, Ga) [27], FeVX (X = As, P) [28] and IrCrZ (Z = Ge, As, Sn, Sb) [29]. Because the energy band gap encompasses a large range of frequencies of electromagnetic waves, from in the range infrared to ultraviolet [30–32], optical characteristics of 2D materials have

been widely explored [33–38]. Because the combination of electrical and optical properties permits the regulation of electronic current or optical transitions with different degrees of freedom, is important in fundamental physics and applications in electronic–photonic systems.

Magneto-electronics, electro-mechanics, and spintronics are just few of possible applications where these materials could be useful. Depending on the dimensionality and the environment, the transition metals are exceptionally significant because they permit interactions of complex magnetic, resulting in fascinating magnetic, magnetoelectric, piezo-electric features [39–41], and the conversion of non-magnetic materials to magnetic materials [42]. A broad scope of electrical, magnetic, and optical characteristics were discovered in previous studies [43]. The electronic, magnetic and optical properties of the TM are mostly determined by the TM 's' unfilled or filled 'd' bands. Half Heusler alloys are unique from the other Heusler alloys that have high Curie temperature and lattice constants are compatible with semiconductor substrates. Optical applications, magnetic tunnel junctions, power storage, semiconductors, lenses, and medicinal applications have all used these materials [44]. A lot of investigations are carried out on the bulk, interface and surface characteristics of half metallic materials [45–49].

In the current study, we studied new LiCrN compound where the structural, electronic, magnetic, and optical properties of LiCrN by means of first-principles calculations based on density func-

Fig. 1. Structure of Heusler compounds LiCrN.

Fig. 2. The overall energy as a function of lattice constants made by half Heusler alloy LiCrN.
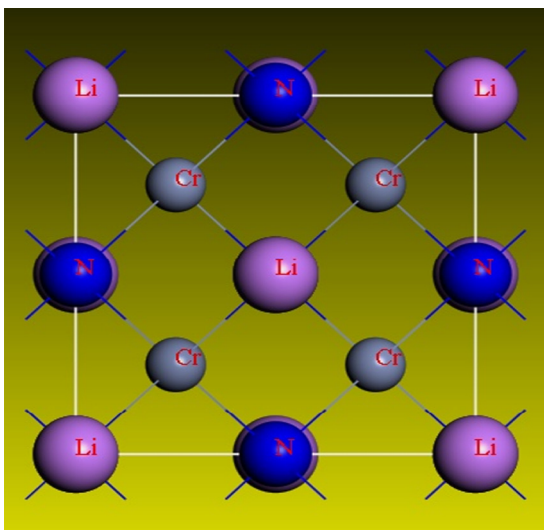
tional theory (DFT) are thoroughly explored. It is found that the half Heusler alloy LiCrN is truly HM ferromagnetic with energy and HM gaps of 3.65 and 0.5 eV, respectively.

2. Computational method

The structural, electrical, magnetic and optical properties of the LiCrN alloy are calculated using the density functional theory (DFT) via employing the CASTEP code [50]. The Perdew–Burke–Ernzerhof (PBE) formulation has been used to describe the exchange-correlation energy based on the generalized gradient approximation (GGA) (PBE-GGA) [51], to obtain accurate band structure for this compound, HSE06 is used. For the most part, integrations of reciprocal space are made using $15 \times 15 \times 15$ k-point meshes of Monkhorst–Pack in the first Brillion zone (1BZ). For all atoms, the smallest value of a muffin sphere radius (R_{mt}) is considered to be 2.5 a.u. for Li, Cr and N. In that calculations, a separation power of 400 eV on a plan-wave basis is used, and the structure is completely at rest with a force acting on the atoms lower than 0.01 eV/Å, and the total energy convergence is 10^{-6} eV. The first Brillion region is sampled by a k-mesh ($15 \times 15 \times 15$) to simulate the structural, electronic, magnetic, and optical properties of LiCrN.

3. Results and discussion

3.1. Bulk structural and electronic properties

The cubic form of LiCrN has a space group of P-43m (216), and the Li, Cr, and N atoms are arranged in one formula unit at a (0, 0, 0), b (0.25, 0.25, 0.25) and c (0.5, 0.5, 0.5) sites of Wyckoff coordinates, respectively, as shown in Fig. 1. Based on the curve of energy as a function to lattice constant it is found that the equilibrium lattice constant is 5.11 Å, as displayed in Fig. 2. Due to the importance of the electronic properties, we study the organization of the electronic band structure for LiCrN in the Brillion zone (BZ). The Heusler alloy band structure of LiCrN reveals a metallic performance in the spin-majority because the bands crossed the Fermi level, while the spin-minority channel semiconductor property within the indirect gap located between Δ (minimum conduction band) and W (maximum valence band) points, see Fig. 3. This means that the LiCrN is an half metallic ferromagnetic material. The indirect gap in the minority spin state is roughly 3.65 eV in (PBE-GGA), and 5.06 eV in (HSE06). Furthermore, the half-metallic gap (HMgap), which is specified as the lowest value between the
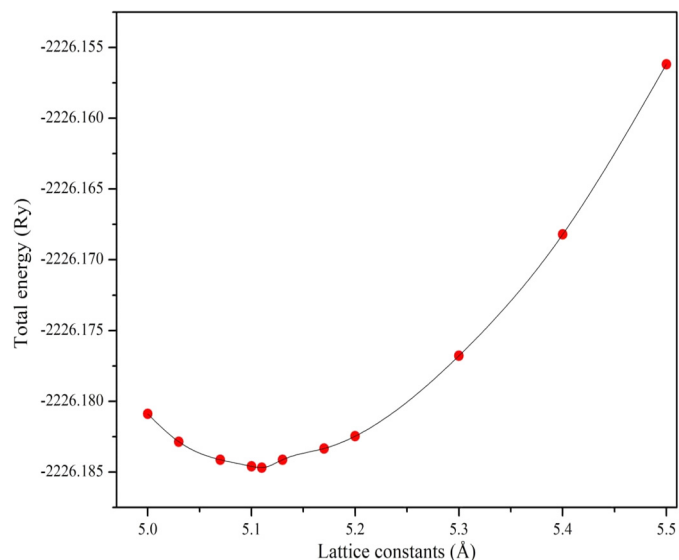
minimum conduction band (MCB)/maximum valence band (MVB) to Fermi level. So HMgap = 0.5 eV. The energy gap and HMgap are significant parameters in the spintronics devices.

3.2. Density of states and magnetic properties

At the equilibrium lattice constant, the total and partial density of states (TDOS and PDOS) of half Heusler alloy LiCrN were considered and exhibited in Fig. 4. TDOS in the valence region below the Fermi level, a maximum peak is found at -3.15 eV due to the main contribution of the Cr atom and the contribution is lower for Li and N atoms. The spin-down state and the Fermi energy level are multiplied by -1 and 0, respectively. The DOS of the marginal spin of the alloy displayed the banned energy gap, with the N states dominating on the valance part of DOS, while the DOS of Li and Cr dominate on the conduction band. In the meantime, for the up spin, the DOS of the LiCrN alloy and Li, Cr, and N DOS peaks to around E_F, evidently signifying metallic conduct of LiCrN majority spin. The alteration in the energy gap values regarding the alteration in the lattice parameter was summarized in this study. Finally, we infer that hybridization between the Cr d-orbit and the N p-orbit is one of the reasons for the emergence of the LiCrN energy band-gap. The Li element's contribution to the total density of states is negligible. When the values of lattice constants increase the energy gap decreases. As a result, the HM characteristic is preserved in this combination. The Cr atom has high contribution with the magnetic qualities indicated by the spin magnetic moment. This is attributed to that the outer shell of the Cr atom has more electrons compared to the other atoms. The Slater-Pauling rule [52,53] is used to compute the total magnetic moment, $M_t = Z_t - 8$, where Z_t is the total electrons in the valence band in the primitive cell, as per the overall number of valence electrons, Li: $2S^1$, Cr: $4S^1 3d^5$, and N: $2S^2 2P^3$, there are 12 valence electrons in LiCrN alloy. Therefore, the total value of spin magnetic moment is determined to be 4.00 μ_B. The spin magnetic moments of Li, Cr, and N are 0.17, 3.49, and -0.14 μ_B respectively and the interstitial area is 0.48 μ_B. The greater impact of the total magnetic moment value is due to the atom of Cr, where a bigger spin magnetic moment emerges matched to the further atoms, whereas the atom N has a tiniest minor impact which might be overlooked.
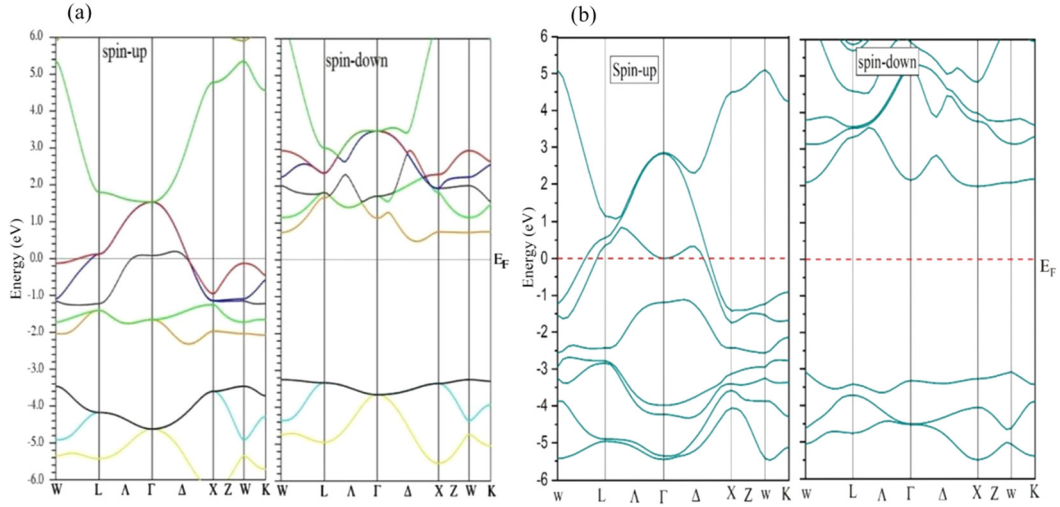
Fig. 3. The spin (up and down) channels of half Heusler alloy LiCrN band structure according to (a) (PBE-GGA) and (b) HSE06. The Fermi level is represented by E_F.
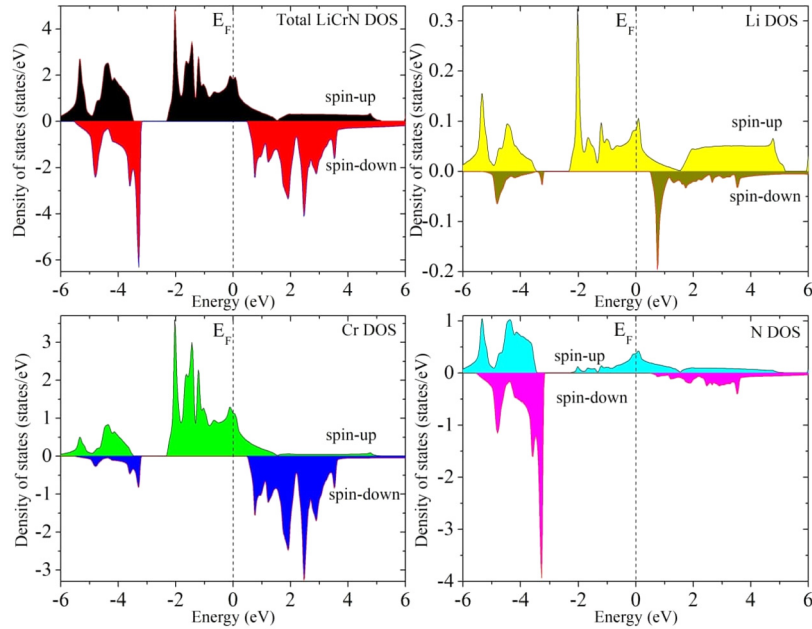

Fig. 4. Total density of state (TDOS) of LiCrN and partial density of states of Li, Cr and N atoms.

3.3. Optical properties

The optical spectra as a function of energy for LiCrN are shown in Fig. 5. The optical properties are studied in the 0–15 eV range of energy. Many applications and practical research require a thorough understanding of the compound's optical characteristics. In order to compute the multifaceted dielectric function that undertakes the self-energy and local field rectifications, it is critical to have an extremely dense grid and an exact exchange correlation in the FP-LAPW. With a $30 \times 30 \times 30$ grid, high precision Trans Blaha-Modified Becke-Johnson is used to calculate the optical properties. The optical constants such as absorption coefficients, reflectivity, refractive index and dielectric function are presented in this section.

We calculate the optical properties including dielectric function, $\varepsilon(\omega)$, absorption coefficient $\alpha(\omega)$, refractive index ($n(\omega)$) and optical reflectivity, $R(\omega)$. $\varepsilon(\omega)$, $n(\omega)$ and propagation constant $k(\omega)$ are written as follows:

$$\varepsilon(\omega) = \varepsilon_r(\omega) + i\varepsilon_I(\omega) \tag{1}$$

$$n(\omega) = \left(\frac{\sqrt{\varepsilon_r^2(\omega) + \varepsilon_I^2(\omega)} + \varepsilon_r(\omega)}{2} \right)^{1/2} \tag{2}$$

$$k(\omega) = \left(\frac{\sqrt{\varepsilon_r^2(\omega) + \varepsilon_I^2(\omega)} - \varepsilon_r(\omega)}{2} \right)^{1/2} \tag{3}$$

Fig. 5 shows the plot of the dielectric function $\varepsilon(\omega)$ vs. photon energy. The transitions of the intra-band and inter-band are the two forms of contributions to the dielectric. The direct and indirect transitions of inter-band are two types of inter-band transition. Because electron excitation by photon across the indirect band gap is comparatively infrequent due to the small photon momentum once matched to the direct transition of inter-band, the indirect transition of inter-band is ignored. It encapsulates the material reaction to (E). The dielectric function is fully reliant on the unoccupied and occupied wave functions attained by evaluating the momentum matrix components; hence the electronic band struc-
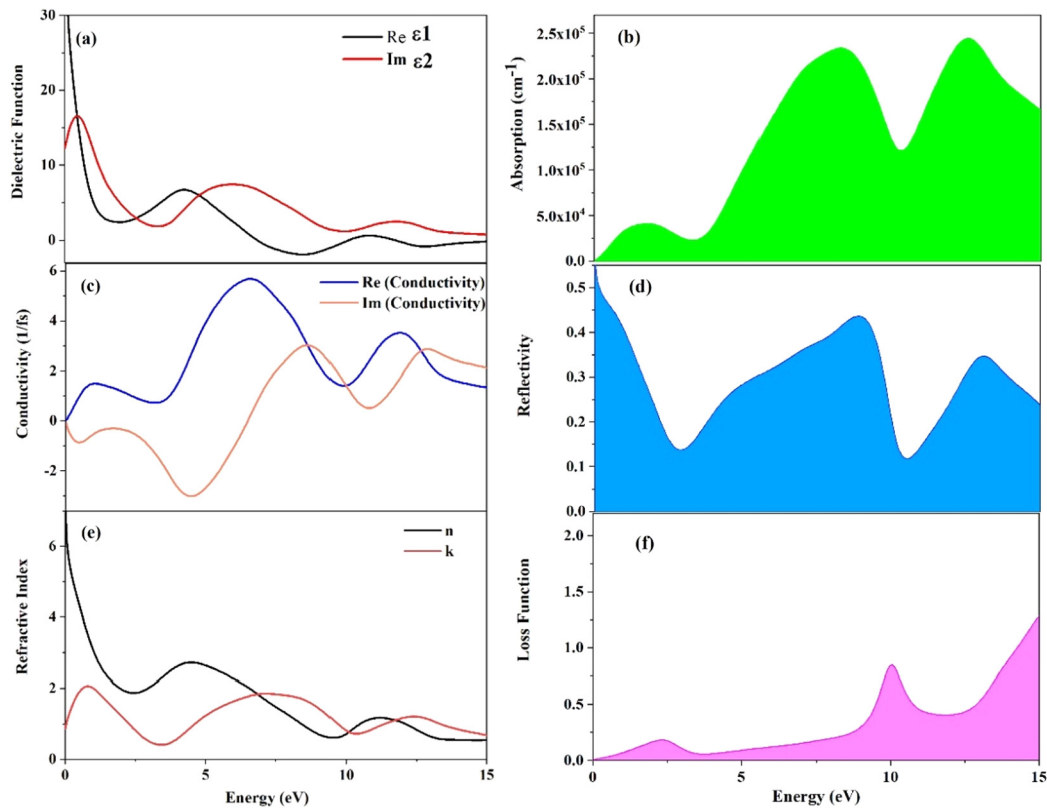
Fig. 5. (a) Real and imaginary parts of the complex dielectric function, (b) Absorption coefficient, (c) Optical conductivity, (d) Optical reflectivity, (e) Refractive index, and (f) Loss function of LiCrN.

ture plays a crucial role in characterizing the function of dielectric. The real part $\varepsilon_r(\omega)$ is related to the propagative behavior of an electromagnetic field. The imaginary part $\varepsilon_I(\omega)$ was produced by summing the transitions of occupied-non occupied by using the rule of Fermi golden [54], and the real part $\varepsilon_r(\omega)$ is consequent from the relation of Kramer-Kronig [55]. Fig. 5 (a) displays the actual and imaginary plots for the dielectric function for the LiCrN alloy in the photon energy range of $0-15$ eV. The static dielectric constant at energy zero is $\varepsilon_r(0) = 30$ for LiCrN. After that, the value of $\varepsilon_r(0)$ tends to be constant. Reflection of incident radiation from the surface is indicated by negative numbers. LiCrN has real part dielectric constant of 15 eV. The zero frequency value of the imaginary component of the dielectric function, ε_I gives the optical band gap of a compound. When the energy is in the 0.0 eV range, the absorption coefficient is nearly nil, and there are no electronic transitions since the photon's energy is less than the band gap of LiCrN. (see Fig. 5 (b)). The absorption coefficient $\alpha(\omega)$ of photon energy is shown in Fig. 5 (b). The absorption features may be seen in the 15 eV range. LiCrN has a maximum absorption coefficient of 243545.6 at 12.6 eV. LiCrN is a wide band gap compound with strong ultraviolet absorption power that can be employed in optoelectronic devices such as UV detectors. Fig. 5 (c) depicts the true (absorptive) part of optical conductivity. We can observe that absorption peaks occur at 1.5, 3.1, and 5.7 for photon energies of 1.5, 12, and 7 eV, and then progressively decrease to zero for high energy photons. The reflectivity $R(\omega)$ is computed using the following formula.

$$R(\omega) = \left| \frac{\sqrt{\varepsilon(\omega)} - 1}{\sqrt{\varepsilon(\omega)} + 1} \right|^2 \tag{4}$$

In the visible range of energy, the reflectivity is highest, and the components could be employed as reflective coatings in this range.

As a result, such spectral band offers good ultraviolet (UV) absorption as well as increased energy absorption. It is widely known that components with band gaps greater than 3.1 eV, such as those used in this study, perform well in the UV part of the spectrum [56]. We find a continuous increase in the compound after 2.6 eV (Fig. 5d). Eqs. (2) and (3) are used to compute the refractive index $n(\omega)$ and the extinction coefficient k(ω), as illustrated in Fig. 5 (e). In the visible portion of the spectrum, high peaks in the refractive index can be seen. The greatest value of the static refractive index $n(\omega)$ is 3.9 at 2.7 eV. The refractive index tends to unity at high photon energy, but it increases and decreases with energy in the IR and visible ranges, respectively. At 0.6 eV, the extinction coefficient reaches its local maximum. In the UV region, the spectrum of $n(\omega)$ and $k(\omega)$ rapidly drops with increasing photon energy and becomes constant after 15 eV. Eq. (5) can be used to calculate the energy lost by the electron.

$$L(\omega) = -\text{Im}\left\{ \frac{1}{\varepsilon(\omega)} \right\} = \left(\frac{\varepsilon_I(\omega)}{\varepsilon_r^2(\omega) + \varepsilon_I^2(\omega)} \right) \tag{5}$$

The plasma resonance behavior is represented by the high peaks in the $L(\omega)$ versus energy plots, and the frequencies at which these peaks form are known as plasma frequency. Fig. 5 (f) shows the behavior of the volume energy loss function as a function of photon energy. It is apparent for the largest extinction to occur at (1.7 eV), indicating that both the energy losses when fast single electrons migrate from valance band to conduction band in the LiCrN sheet occur at this level.

4. Conclusion

In summary, the electronic, magnetic and half metallic characteristics of the LiCrN compound in a space group of P-43m (216)

is investigated using the first-principle calculations. The calculated band structure shows the half metallic property for LiCrN alloy. Where it is a semiconductor with band gap (3.65 eV) and insulator due to large band gap (5.06 eV) according to (PBE-GGA) and (HSE06), respectively in spin down channel. The spin-down channel has an energy gap of 3.65 eV. The HMgap is 0.5 eV. The total magnetic moment is 4.00 μ_B which is in worthy compliance with Slater–Pauling's rule. The Cr atom contributes the most to the overall magnetic moment, while the contribution of other atoms is low. Furthermore, we investigate the optical properties because one of the spin channels has semiconductor characteristics, making it a candidate for optoelectronics devices. The results indicate that this structure could be useful in spintronics applications.

CRediT authorship contribution statement

Ammar A. Kadhim: Data curation, Formal analysis, Software, Writing – original draft. **Jabbar M. Khalaf Al-zyadi:** Writing – review & editing, Writing – original draft, Software, Methodology, Investigation, Formal analysis, Data curation, Conceptualization, Resources. **Maged A. Nattiq:** Writing – original draft, Investigation, Formal analysis, Data curation.

Declaration of competing interest

The authors declare that they have no known competing financial interests or personal relationships that could have appeared to influence the work reported in this paper.

References

[1] T. Dietl, H. Ohno, F. Matsukura, J. Cibert, D. Ferrand, Science 287 (2000) 1019.
[2] R.A. de Groot, F.M. Mueller, P.G. van Engen, K.H.J. Buschow, Phys. Rev. Lett. 50 (1983) 2024.
[3] E. Şaşıoğlu, L.M. Sandratskii, P. Bruno, I. Galanakis, Phys. Rev. B 72 (2005) 184415.
[4] I. Galanakis, P.H. Dederichs, N. Papanikolaou, Phys. Rev. B 66 (2002) 174429.
[5] O. Amrich, Mohammed El Amine Monir, H. Baltach, S. Bin Omran, Xiao-Wei Sun, Xiaotian Wang, Y. Al-Douri, A. Bouhemadou, R. Khenata, J. Supercond. Nov. Magn. 31 (2018) 241.
[6] M. Ayad, F. Belkharroubi, F.Z. Boufadi, M. Khorsi, M.K. Zoubir, M. Ameri, I. Ameri, Y. Al-Douri, K. Bidai, D. Bensaid, Indian J. Phys. 94 (2020) 767.
[7] B. Fadila, M. Ameri, D. Bensaid, M. Noureddine, I. Ameri, S. Mesbah, Y. Al-Douri, J. Magn. Magn. Mater. 448 (2018) 208.
[8] F. Khelfaoui, M. Ameri, D. Bensaid, I. Ameri, Y. Al-Douri, J. Supercond. Nov. Magn. 31 (2018) 241.
[9] A. Mentefa, F.Z. Boufadi, M. Ameri, F. Gaid, L. Bellagoun, A. Abu Odeh, Y. Al-Douri, J. Supercond. Nov. Magn. 34 (2021) 269.
[10] D. Bensaid, T. Hellal, M. Ameri, Y. Azzaz, B. Doumi, Y. Al-Douri, B. Abderrahim, F. Benzoudji, J. Supercond. Nov. Magn. 29 (2016) 1843.
[11] A. Moussali, M.B. Amina, B. Fassi, I. Ameri, M. Ameri, Y. Al-Douri, Indian J. Phys. 94 (2020) 1733.
[12] Y. Ji, G.J. Strijkers, F.Y. Yang, C.L. Chien, J.M. Byers, A. Anguelouch, G. Xiao, A. Gupta, Phys. Rev. Lett. 86 (2001) 5585.
[13] F.J. Jedema, A.T. Filip, B.J. van Wees, Nature 410 (2001) 345.
[14] T. Shishidou, A.J. Freeman, R. Asahi, Phys. Rev. B 64 (2001) 180401.
[15] Y. Tomioka, T. Okuda, Y. Okimoto, R. Kumai, K.I. Kobayashi, Y. Tokura, Phys. Rev. B 61 (2000) 422.
[16] J.H. Park, E. Vescovo, H.J. Kim, C. Kwon, R. Ramesh, T. Venkatesan, Nature 392 (1998) 794.
[17] L. Kronik, M. Jain, J.R. Chelikowsky, Phys. Rev. B 66 (2002) 041203.
[18] Y. Liu, B.-G. Liu, J. Phys. D 40 (2007) 6791.
[19] H. Pan, Y.P. Feng, Q.Y. Wu, Z.G. Huang, J. Lin, Phys. Rev. B 77 (2008) 125211.
[20] K.L. Yao, G.Y. Gao, Z.L. Liu, L. Zhu, Y.L. Li, Physica B 366 (2005) 62.
[21] L. Damewood, B. Busemeyer, M. Shaughnessy, C.Y. Fong, L.H. Yang, C. Felser, Phys. Rev. B 91 (2015) 064409.
[22] X. Wang, Z. Cheng, G. Liu, Materials 10 (2017) 1078.
[23] R. Ahmad, N. Mehmood, S. Bukhari, W. Nafees, M. Arif, J. Supercond. Nov. Magn. 31 (2018) 2617.
[24] M. Moradi, N. Taheri, M. Rostami, Phys. Lett. A 382 (2018) 3004.
[25] N. Mehmood, R. Ahmad, G. Murtaza, J. Supercond. Nov. Magn. 30 (2017) 2481.
[26] M. Ameri, A. Touiaa, R. Khenata, Y. Al-Douri, H. Baltache, Optik 124 (2013) 570.
[27] A. Missoum, T. Seddik, G. Murtaza, R. Khenata, A. Bouhemadou, Y. Al-Douri, A. Abdiche, H. Meradji, H. Baltache, Can. J. Phys. 92 (2014) 1.
[28] N. Chami, O. Arbouche, S. Chibani, F.-Z.D. Khodja, K. Amara, M. Ameri, Y. Al-Douri, M. Adjdir, J. Electron. Mater. 49 (2020) 4916.
[29] M.A. Behbahani, M. Moradi, M. Rostami, S. Davatolhagh, J. Phys. Chem. Solids 92 (2016) 85.
[30] K.F. Mak, L. Ju, F. Wang, T.F. Heinz, Solid State Commun. 152 (2012) 1341.
[31] F. Bechstedt, L. Matthes, P. Gori, O. Pulci, Appl. Phys. Lett. 100 (2012) 261906.
[32] A. Zunger, A. Katzir, A. Halperin, Phys. Rev. B 13 (1976) 5560.
[33] A. Bafekry, I.A. Sarsari, M. Faraji, M.M. Fadlallah, H.R. Jappor, S. Karbasizadeh, V. Nguyen, M. Ghergherehch, Appl. Phys. Lett. 118 (2021) 143102.
[34] A. Bafekry, S. Karbasizadeh, C. Stampfl, M. Faraji, D.M. Hoat, I. Abdolhosseini Sarsari, S.A.H. Feghhia, M. Ghergherehchih, Phys. Chem. Chem. Phys. 23 (2021) 15216.
[35] A. Bafekry, C. Stampfl, M. Faraji, M. Yagmurcukardes, M.M. Fadlallah, H.R. Jappor, M. Ghergherehchi, S.A.H. Feghhi, Appl. Phys. Lett. 118 (2021) 203103.
[36] A. Bafekry, M. Faraji, N.N. Hieu, Y.S. Ang, S. Karbasizadeh, I. Abdolhosseini Sarsari, M. Ghergherehchi, Nanotechnology 33 (2021) 075707.
[37] A. Bafekry, M. Faraji, S. Karbasizadeh, I.A. Sarsari, H.R. Jappor, M. Ghergherehchi, D. Gogova, Phys. Chem. Chem. Phys. 23 (2021) 24336.
[38] A. Bafekry, M. Faraji, M.M. Fadlallah, I.A. Sarsari, H.R. Jappor, S. Fazeli, M. Ghergherehchi, Appl. Phys. Lett. 119 (2021) 142102.
[39] A.A. Ramanathan, J.M. Khalifeh, J. Magn. Magn. Mater. 426 (2017) 450.
[40] H. Cai, Y. Guo, H. Gao, W. Guo, Nano Energy 56 (2019) 33.
[41] J.T. Wang, C. Zhang, Ferroelectrics 301 (2004) 211.
[42] A.A. Ramanathan, J.M. Khalifeh, B. Hamad, J. Magn. Magn. Mater. 321 (2009) 3804.
[43] M.V. Kovalenko, L. Protesescu, M.I. Bodnarchuk, Science 358 (2017) 745.
[44] A.A. Mubarak, A.A. Mousa, Comput. Mater. Sci. 59 (2012) 6.
[45] J.M. Khalaf Al-zyadi, N.H. Abdul-Wahhab, K.L. Yao, K.L. Yao, J. Magn. Magn. Mater. 446 (2018) 221.
[46] J.M. Khalaf Al-zyadi, R.M. Samuel, K.L. Yao, J. Magn. Magn. Mater. 346 (2013) 166.
[47] J.M. Khalaf Al-zyadi, G.Y. Gao, K.L. Yao, Thin Solid Films 531 (2013) 266.
[48] G.Y. Gao, W. Yao, H.P. Han, J.M. Khalaf Al-zyadi, K.L. Yao, J. Appl. Phys. 112 (2012) 103709.
[49] J.M. Khalaf Al-zyadi, G.Y. Gao, K.L. Yao, Comput. Mater. Sci. 86 (2014) 140.
[50] S.J. Clark, M.D. Segall, C.J. Pickard, P.J. Hasnip, M.I. Probert, K. Refson, M.C. Payne, First principles methods using CASTEP, Z. Krist. 220 (2005) 567.
[51] J.P. Perdew, K. Burke, M. Ernzerhof, Phys. Rev. Lett. 77 (1996) 3865.
[52] J.C. Slater, Phys. Rev. 49 (1936) 931.
[53] L. Pauling, Phys. Rev. 54 (1938) 899.
[54] G.Y. Guo, K.C. Chu, D.S. Wang, C.G. Duan, Phys. Rev. B 69 (2004) 205416.
[55] M. Gajdoš, K. Hummer, G. Kresse, J. Furthmüller, F. Bechstedt, Phys. Rev. B 73 (2006) 045112.
[56] M. Maqbool, B. Amin, I. Ahmad, J. Opt. Soc. Am. B 26 (2009) 2180.